

Flows in out-phase slip-patterned micro-channels using boundary element methods

*Chandra Shekhar Nishad¹, Anirban Chandra², and G.P. Raja Sekhar¹

¹Department of Mathematics, Indian Institute of Technology Kharagpur, India.

²Department of Mechanical Engineering, Indian Institute of Technology Kharagpur, India

*Presenting & Corresponding author: csnishad@maths.iitkgp.ernet.in

Abstract

Flow through two-dimensional rectangular micro-channel with patterned slip on the walls under the low-Reynolds number limit ($Re \ll 1$) is studied using boundary element method (BEM). We assume that the pattern of the slip on the upper and the lower walls maintain a phase difference (i.e., out-phase configuration). We considered two subcases of out-phase patterned slip, namely large and fine depending on the characteristic length of the patterning. In order to obtain a deep insight of flow mechanics, we investigated the streamlines, velocity profiles, shear stress, and pressure gradients with varying slip-length (l_s).

Keywords: Stokes equation, micro-channel, slip patterning, boundary element method.

Introduction

In order to model the flow of a viscous incompressible fluid over solid boundaries, proper understanding about the boundary conditions at the interface of solid and liquid are required. The most applicable boundary condition is the no-slip condition which generally state that the fluid velocity at the wall is equal to the wall velocity. The no-slip boundary condition does not work in certain occasions like flows over hydrophobic surfaces, problems involving multiple interfaces, and flow of rarefied fluids. In the past, several researchers have proposed various models to correctly defines the interaction between a solid wall and a liquid. A detailed discussion about the slip boundary condition can be found in [1].

The range of slip-length is affected by several factors. A perfect slip (large slip) can be observed in situations where the nanobubbles are trapped over hydrophobic surfaces. In most of the micro-fluidic applications, there is a high possibility of encountering the irregular boundaries. In order to handle such complex boundary conditions, attempting analytical solution might be impossible. In that case one has to rely on numerical solution.

There are several domain discretization techniques (such as finite difference method (FDM), finite element method (FEM), and finite volume method (FVM)) available in literature to solve such fluid flow problems involving complex boundaries. In case of linear operators another technique available in literature which is based on the integral equation method known as boundary element method (BEM). The major advantage of this technique over the others is that the dimension of the solution domain is reduced by order one, which results in saving computational resources.

Understanding flow through rectangular micro-channels is useful in designing and optimization of lab on chips systems. At the micro, and nano length scales, the ability to fabricate patterns and structures has produced a board area of scientific research. The interaction between solid wall and liquid defines slip or no-slip conditions on a wall. The hydrophilic and hydrophobic surfaces are characterized by no-slip and partial slip boundary conditions. In order to design hydrophobic/hydrophilic surfaces, various investigations on chemical modification of surfaces have been done ([2] [3]). In this connection, surfaces coated with alternate slip and no-slip are important in reducing drag [4]. The ability to manipulate the flow to enhance the mixing in the low-Reynolds number limit is another very interesting phenomena of the surfaces coated with alternate slip and no-slip boundary conditions. In [1], the idea of in-phase patterned slip has been used, while studying Stokes flow in a two-dimensional rectangular micro-channels. In this study, we extend the work of [1] by considering the out-phase configuration of patterned slip in rectangular micro-channels.

Mathematical Formulation

Let us consider a steady, two-dimensional, viscous incompressible Newtonian flow at low Reynolds number that is governed by Stokes equation together with the continuity equation given by the respective non-dimensional form,

$$\nabla P = \nabla^2 \mathbf{U}, \quad \nabla \cdot \mathbf{U} = 0, \quad (1)$$

where the non dimensionalization is done using the characteristic variables,

$$\mathbf{U} = \frac{\mathbf{u}}{\tilde{U}}, \quad \mathbf{X} = \frac{\mathbf{x}}{L}, \quad P = \frac{pL}{\mu \tilde{U}}.$$

Eliminating the pressure term from Eq. (1) while introducing stream function, Stokes equation can be reduced to a biharmonic equation which is given by,

$$\nabla^4 \psi = 0. \quad (2)$$

In order to solve Eq. (2) using boundary element method, the biharmonic equation is rewritten as a coupled system of Poisson and Laplace equation in terms of stream function-vorticity variables,

$$\nabla^2 \psi = -\omega, \quad \nabla^2 \omega = 0. \quad (3)$$

In order to solve Eq. (3) we use direct biharmonic boundary integral equation methods (BBIE). Of course one may recall boundary integral formulation based on velocity-traction variables [15]. However, here we restrict to stream function-vorticity formulation without debating much on the relative advantages and disadvantages. In the literature, several authors have reviewed the BBIE methods ([5]-[13]) in significant detail. Therefore, in this study we present this method in brief. Let us denote a general field point by $p(X, Y)$ and an integration point on the boundary by $q(X_0, Y_0)$, so that $p \in \Omega \cup \partial\Omega$ and $q \in \partial\Omega$. Let G^L and G^B be the fundamental solutions

corresponding to Laplacian and biharmonic operators which satisfies $\nabla^2 G^L = \delta(|q-p|)$, and $\nabla^4 G^B = \delta(|q-p|)$, where δ is the dirac delta function and $G^L = \log |p-q|$, and $G^B = |p-q|^2 (\log |p-q| - 1)$ [14].

Application of Green's second identity to Eq. (3) gives rise to the following pair of integral equations at a general field point p ,

$$\begin{aligned} \lambda(p)\psi(p) &= \int_{\partial\Omega} [\psi(q) \frac{\partial G^L(p,q)}{\partial n_q} - G^L(p,q) \frac{\partial \psi(q)}{\partial n_q}] ds(q) \\ &\quad - \frac{1}{4} \int_{\partial\Omega} [\omega(q) \frac{\partial G^B(p,q)}{\partial n_q} - G^B(p,q) \frac{\partial \omega(q)}{\partial n_q}] ds(q), \end{aligned} \quad (4)$$

$$\lambda(p)\omega(p) = \int_{\partial\Omega} [\omega(q) \frac{\partial G^L(p,q)}{\partial n_q} - G^L(p,q) \frac{\partial \omega(q)}{\partial n_q}] ds(q), \quad (5)$$

where, $\lambda(p)$ is defined by,

$$\lambda(p) = \begin{cases} 2\pi, & \text{if } p \in \Omega, \\ \pi, & \text{if } p \in \partial\Omega, \\ 0, & \text{if } p \notin \Omega \cup \partial\Omega. \end{cases} \quad (6)$$

We discretized the boundary $\partial\Omega$ into N constant elements $\partial\Omega_j$ containing the mid-element boundary nodes q_j ($j=1,2,\dots,N$). We use piecewise constant functions ψ_j , $\frac{\partial \psi_j}{\partial n}$, ω_j , and $\frac{\partial \omega_j}{\partial n}$, for $j=1,2,\dots,N$ to approximate the values of ψ , $\frac{\partial \psi}{\partial n}$, ω , and $\frac{\partial \omega}{\partial n}$ over each element. Applying the discretized form of Eqs. (4) and (5) at the mid-point $p \equiv q_i \in \partial\Omega_i$ ($i=1,2,\dots,N$) of each element, gives a system of linear equations,

$$A_{ij}\psi_j + B_{ij} \frac{\partial \psi_j}{\partial n_q} + C_{ij}\omega_j + D_{ij} \frac{\partial \omega_j}{\partial n_q} = 0, \quad (7)$$

$$A_{ij}\omega_j + B_{ij} \frac{\partial \omega_j}{\partial n_q} = 0, \quad (8)$$

where the coefficients A_{ij} , B_{ij} , C_{ij} , and D_{ij} are given by,

$$\begin{aligned} A_{ij} &= \int_{q \in \partial\Omega_j} \frac{\partial G^L(q_i, q)}{\partial n_q} ds(q) - \lambda_j \delta_{ij}, & C_{ij} &= -\frac{1}{4} \int_{q \in \partial\Omega_j} \frac{\partial G^B(q_i, q)}{\partial n_q} ds(q), \\ B_{ij} &= -\int_{q \in \partial\Omega_j} G^L(q_i, q) ds(q), & D_{ij} &= \frac{1}{4} \int_{q \in \partial\Omega_j} G^B(q_i, q) ds(q). \end{aligned}$$

where δ_{ij} denotes the Kronecker delta function. In this paper, we use the analytical expression of the above integrals derived by [5]. On solving Eqs. (7) and (8), one obtain the unknown set of boundary variables at each node $q_j \in \partial\Omega_j$, $j=1,2,\dots,N$. Subsequently, one can obtain the values of ψ and ω at a general field point $p \in \Omega$ by solving the Eqs. (7) and (8) for $\lambda(p) = 2\pi$.

Once the values of stream function (ψ) and vorticity (ω) are known inside the domain, one can compute the velocity profiles and pressure gradients by taking their appropriate spatial derivatives, and also evaluate wall shear stress. please refer [1] for details.

Results and Discussion

In this study, we have considered out-phase patterned slip in rectangular micro-channels (see Figs. 1 and 8). Based on the characteristic length of the patterning, we further considered two subcases namely large and fine patterns. When the characteristic length of the patterning (a) is bigger than the width of the channel, we have large patterning, while fine patterning arises when the characteristic length of patterning (a) is smaller than the width of the channel. Depending on the location of the slip or no-slip surface, the boundary conditions are used as follows,

$$\begin{aligned}
 \text{On the top wall (no slip surface)} & : \psi = 1, \frac{\partial\psi}{\partial Y} = 0 : (NS) \\
 \text{On the top wall (slip surface)} & : \psi = 1, \frac{\partial\psi}{\partial Y} + l_s \omega = 0 : (S) \\
 \text{On the bottom wall (no slip surface)} & : \psi = 0, \frac{\partial\psi}{\partial Y} = 0 : (NS) \\
 \text{On the bottom wall (slip surface)} & : \psi = 0, \frac{\partial\psi}{\partial Y} - l_s \omega = 0 : (S) \\
 \text{Inlet} & : \psi = 3Y^2 - 2Y^3, \omega = 12Y - 6 \\
 \text{Outlet} & : \frac{\partial\psi}{\partial X} = 0, \frac{\partial\omega}{\partial X} = 0
 \end{aligned}$$

where l_s represents the dimensionless slip length.

In the present study, we use 240 constant elements to discertize the boundary in a counter-clockwise sense.

Out-phase patterned slip

Here, we consider out-phase configuration of slip-patterning in rectangular micro-channels (see Figs. 1 and 8). The length and width of the channels are 10 and 1 units respectively. The no-slip and slip boundary conditions on the channel wall are characterized by black and grey line segments on the wall. The value of periodicity (a) is same for both the no-slip and slip regime. $a = 2.5$ represents the large patterning, while $a = 0.5$ corresponds to fine patterning. To ignore the effects of inlet and outlet in our discussion we present the results for a certain part of the channel. The two subcases of out-phase slip-patterning (large and fine) have been discussed below.

Large Patterning

In this case, the periodicity of patterning (a) is taken as 2.5 (refer Fig. 1). Fig. 2 shows the contour plots of the streamlines for different values of l_s ranging from 0.1 to 10. It is observed that the streamline profiles look qualitatively similar for different values of l_s .

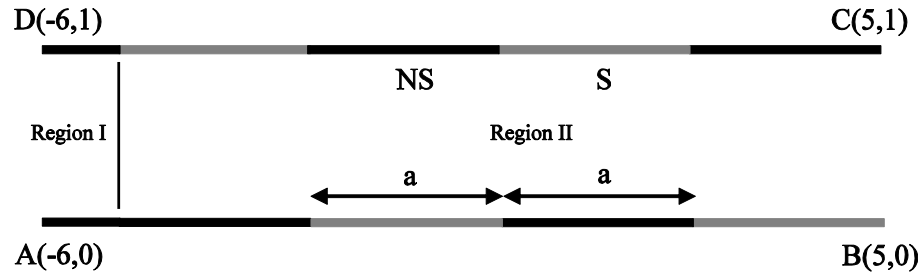


Figure 1. Schematic of the rectangular channel with out-phase large patterned slip. Region I denotes the extension, which is introduced to match the inlet boundary condition. Region II is the actual channel through which the flow is desired.

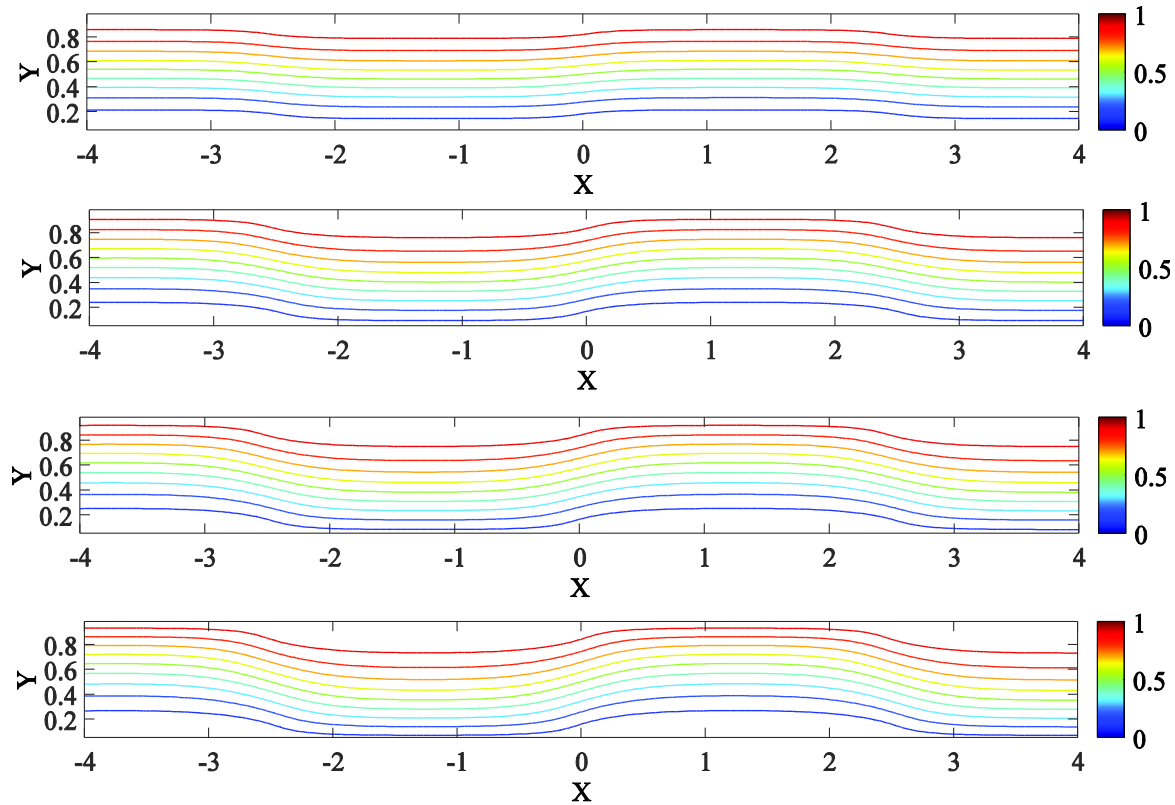


Figure 2. Contour plots of the streamlines for out-phase large patterned slip in rectangular channels with different values of $l_s = 0.1, 0.5, 1$ and 10 .

The variation of the horizontal (U) and vertical (V) velocities with X at $Y = 0.5$ are shown in Fig. 3. The U velocity has significant dependency on the slip-length : with decreasing l_s the value of U at $Y = 0.5$ becomes almost constant (similar to the case where complete no-slip boundary condition is applied on both the walls). On the other hand with increasing l_s , the overall center-line velocity decreases. This fact can be understood on the basis of principle of mass conservation. Interestingly, the maximum U for a particular l_s is attained at the points where a change in boundary conditions take place, i.e., at $X = -2.5, 0$ and 2.5 . The variation of V with X at $Y = 0.5$ is also a function of l_s and its maximum value increases as l_s increases. Moreover the peaks in V are obtained where there is a change of boundary conditions. Similar variation has been observed in the V velocity with X at other values of Y .

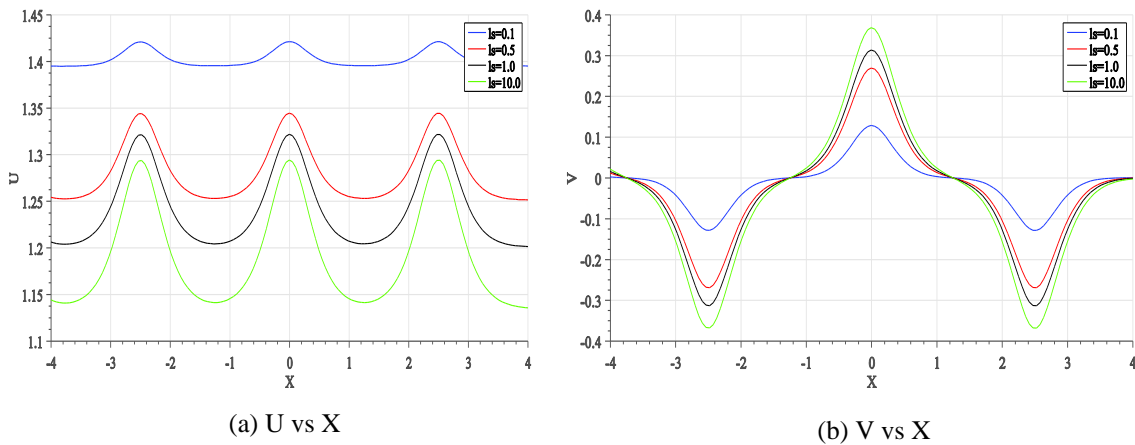


Figure 3. Variation of the horizontal (U) and vertical (V) velocities with X at $Y = 0.5$ for varying slip-length l_s from 0.1 to 10.

In order to gain a proper understanding of the effect of patterns on the walls, U is plotted against X for $Y = 0.05$ and 0.95 , see Fig. 4. It is observed that in the no-slip regime, the effect of the slip-length is not that prominent, and thus U does not seem to vary much with l_s as opposed to the slip-regime where a prominent variation with l_s is noted. In fact when l_s is significantly large then the value of U approaches 1.5, which is theoretically the maximum velocity possible for a channel flow, with the particular inlet conditions that we have utilized. Furthermore, for a particular value of l_s , the U velocity profiles presented in Figs. 4 (a) and 4 (b) are completely out of phase. This is simply because of the fact that the patterning is out of phase, and near the boundaries the flow profiles closely replicate the boundary conditions implemented at the walls.

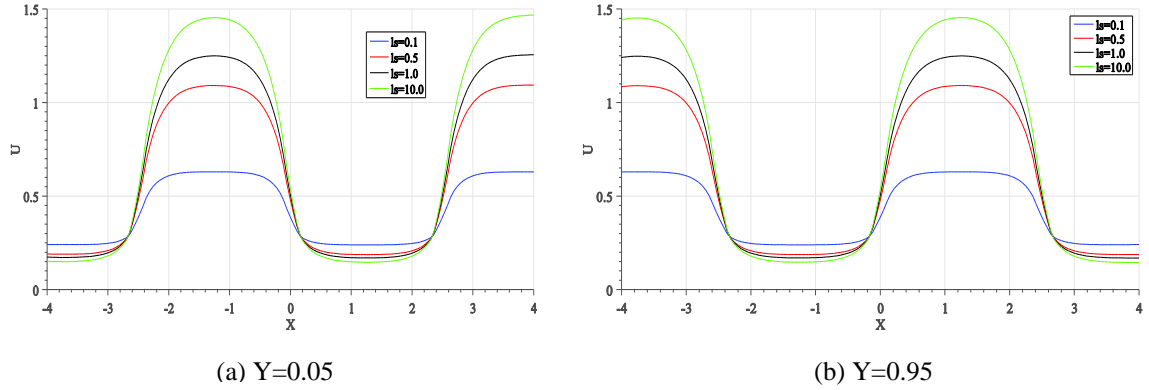


Figure 4. Variation of the horizontal velocity (U) with X at two different values of Y for varying slip length, l_s , from 0.1 to 10.

The variation of U with Y , presented in Fig. 5, shows that at the no-slip end, the U velocity tends to zero and in the slip regime the horizontal velocity varies according to the slip-length. Another interesting fact is that, in Figs. 5 (a) and 5 (b), there exist a particular value of Y for which the U velocity remains the same with varying l_s .

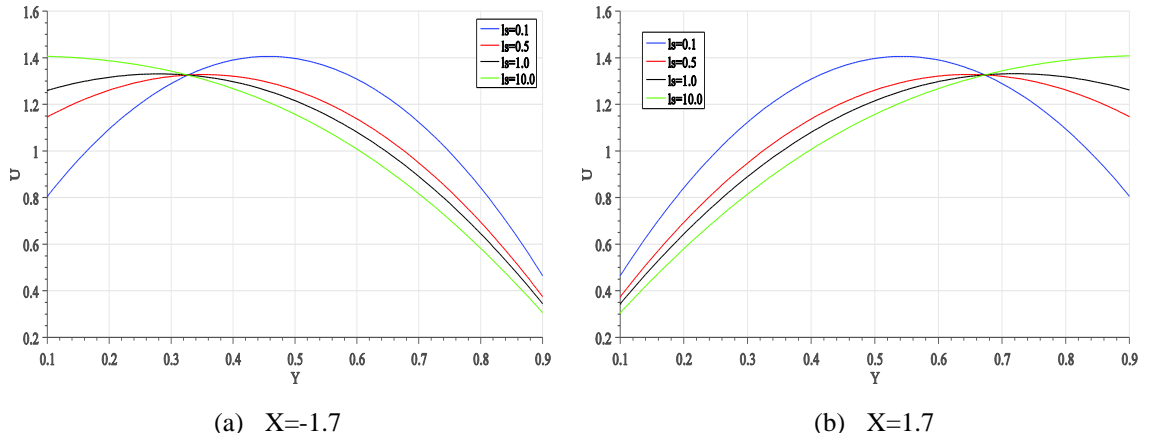


Figure 5. Variation of the horizontal velocity (U) with Y at two different values of X for varying slip length, l_s , from 0.1 to 10.

In order to understand the effect of pressure drop, the variation of pressure gradients (PG) in X -direction against the horizontal distance X at the channel center-line with varying l_s is plotted in Fig. 6. Dips in the pressure gradient (PG) profile are observed at the places where the boundary condition changes. Also, when the slip-length is very low ($l_s = 0.1$ almost represents the no-slip condition) the value of PG tends to a constant value, i.e., the amplitude of variation of PG is reduced. With increasing slip-length there is a net upward shift (tending towards zero) of the PG profile which is justified because, as the slip-length increases there is less resistance to the flow and thus a smaller pressure gradient would be sufficient to drive the flow.

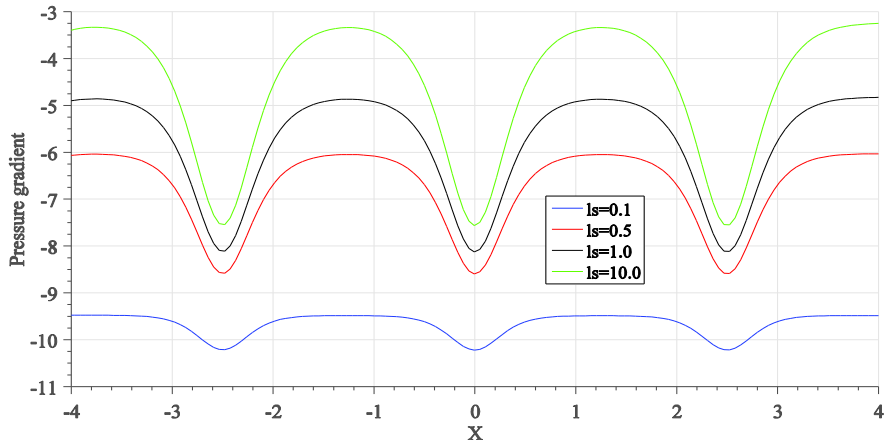


Figure 6. Plot of the pressure gradient (PG) in the X direction with X at $Y = 0.5$ for varying l_s , from 0.1 to 10.

The shear stress on the top wall ($Y = 1$) is plotted with X in Fig. 7. In the slip regime for large value of slip-length ($l_s = 10$) shear stress vanishes on the wall, while in the no-slip regime there is a small variation in the shear stress profiles.

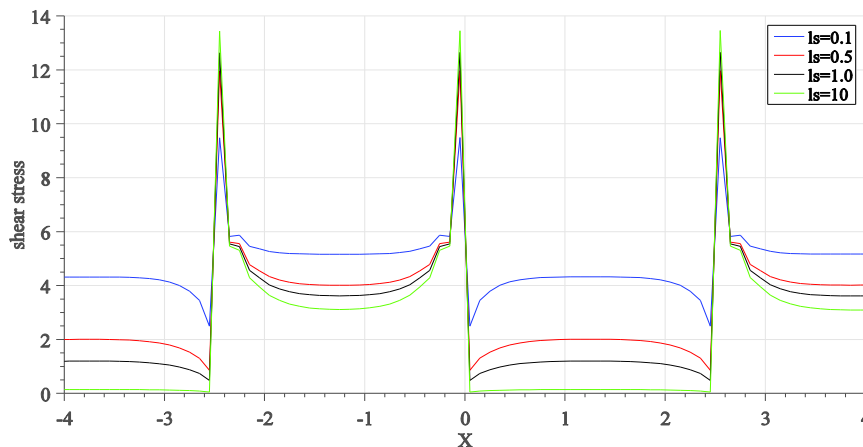


Figure 7. Plot of the shear stress with X at $Y = 1$ for varying l_s , from 0.1 to 10.

Fine Patterning

In this case $a = 0.5$ as shown in Fig. 8. It is observed from Fig. 9 that the streamline profiles remain qualitatively same with varying l_s .

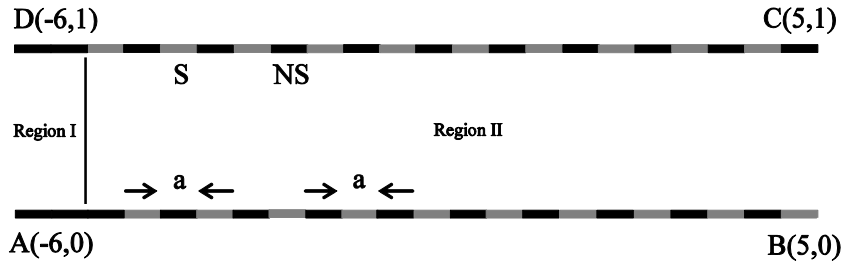


Figure 8. Schematic of the rectangular channel with out-phase fine patterned slip. Region I denotes the extension, which is introduced to match the inlet boundary condition. Region II is the actual channel through which the flow is desired.

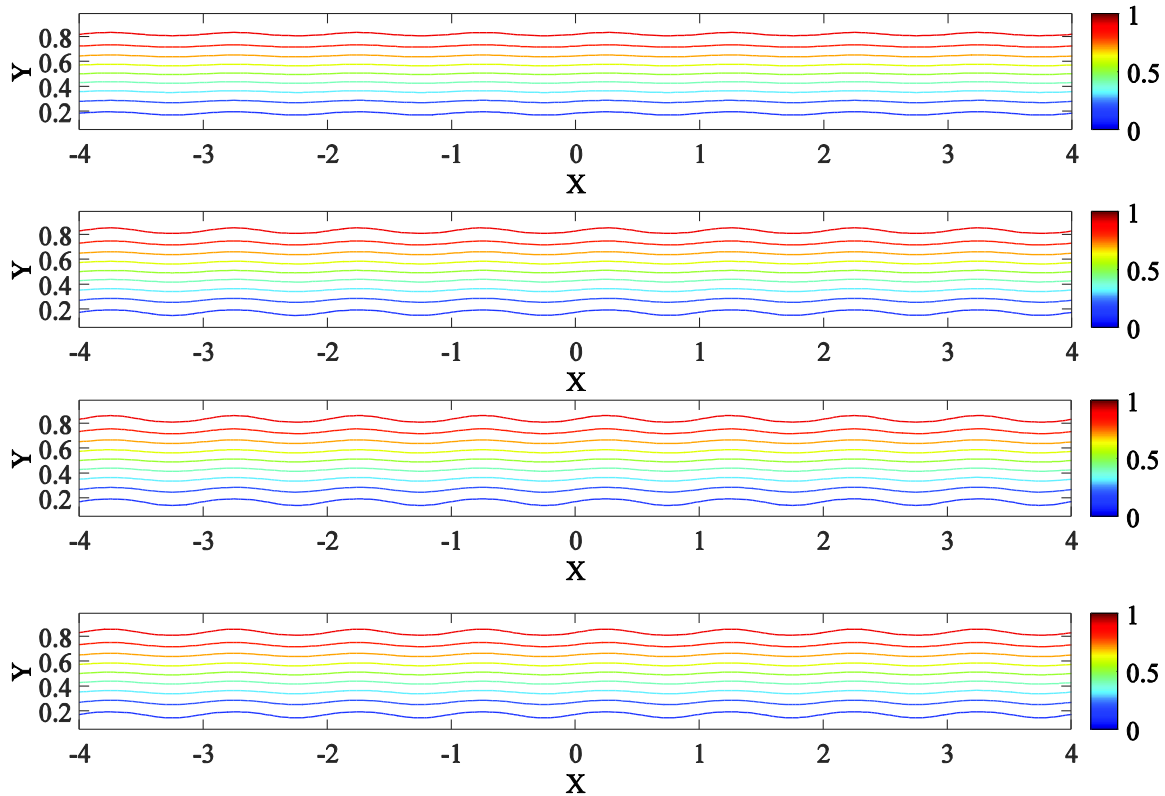


Figure 9. Contour plots of streamline for out-phase fine patterned slip in rectangular micro-channels with different values of $l_s = 0.1, 0.5, 1$ and 10 .

The U and V velocities are plotted with X in Fig. 10. The U velocity has greater dependency over the slip-length l_s . As opposed to the earlier case of out-phase large patterned slip, the amplitude of variation of U is very marginal. This is mainly because of the fact that the characteristic length of patterning is very small which does not let the flow develop as in the previous case. Also, with increase in l_s the center-line U velocity decreases. This fact can be

understood on the basis of principle of mass conservation. From Fig. 10 (b) it is recognized that the variation in V velocity with X is quite similar to the previous case of out-phase large patterned slip but there is a remarkable difference in the magnitude of the variation.

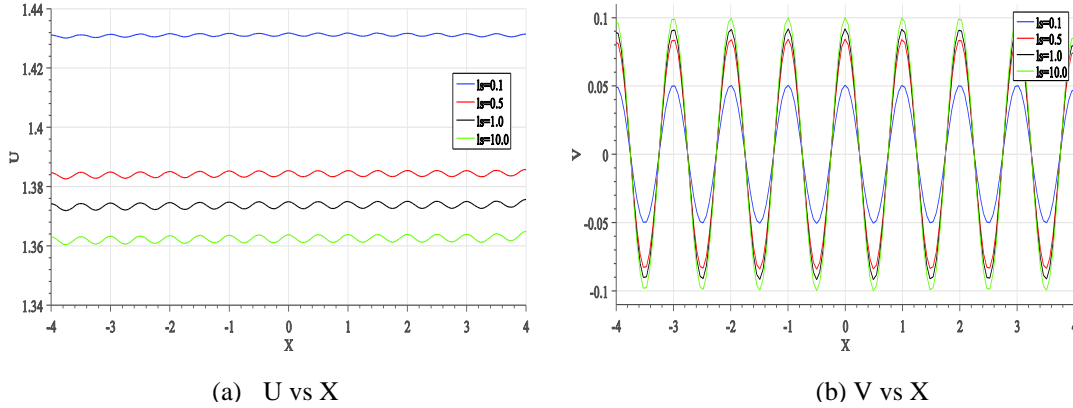


Figure 10. Variation of the horizontal (U) and vertical (V) velocities with X at $Y = 0.5$ for different values of l_s , ranging from 0.1 to 10.

To understand the effect of the boundaries, the variation of U with X at $Y = 0.05$ and 0.95 is shown in Fig. 11. In the slip-regime a prominent variation with l_s is observed, more the slip-length more is the U velocity. Interestingly, when l_s is significantly large, in contrary to the case of large out-phase slip, the value of U does not approach 1.5. The reason for this is that because of the small characteristic length a the flow does not develop fully. In Fig. 11, it can be clearly seen that the U velocity profile at $Y = 0.05$ and $Y = 0.95$ are completely out of phase for varying slip length $l_s = 0.1, 0.5, 1$, and 10 .

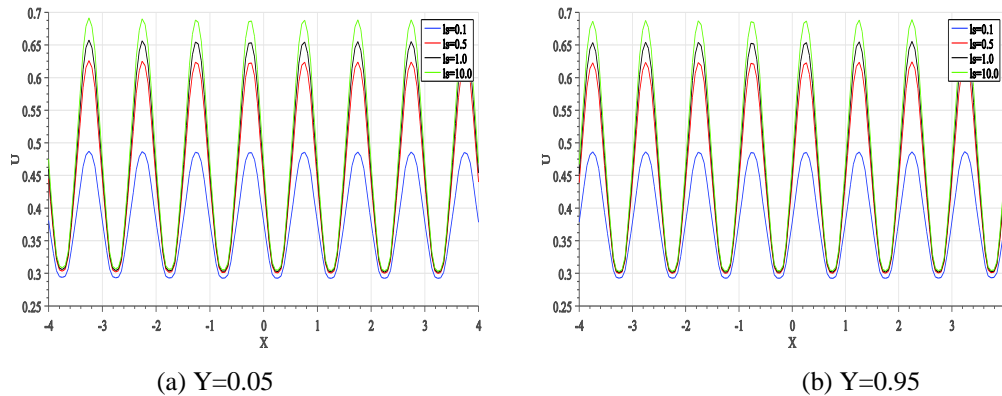


Figure 11. Variation of the horizontal velocity (U) with X at two different values of Y for varying slip length, l_s , from 0.1 to 10.

The U velocity with Y at two different values of X is plotted in Fig. 12. Similar variation in U velocity is observed as in the case of out-phase large patterning, but there is marked difference in U velocity close to the boundary as there is no prominent variation in this

component with l_s .

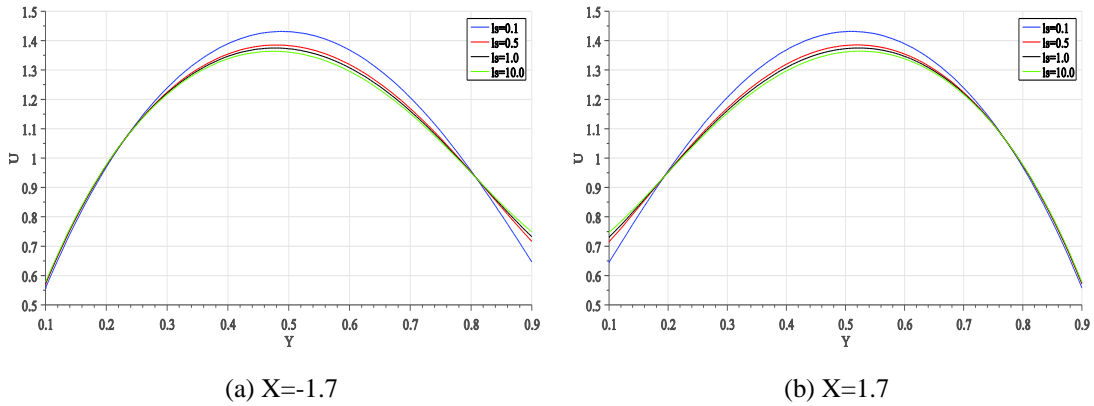


Figure 12. Variation of the horizontal velocity (U) with Y at two different values of X for varying slip-length l_s , from 0.1 to 10.

To clarify the effect of pressure, the variation of the pressure gradient (PG) in the X direction with X is plotted for $Y = 0.5$ (Fig. 13). Due to the small characteristic length of patterning the pressure gradient profile deviates and fluctuates with a smaller amplitude as compared to the previous case.

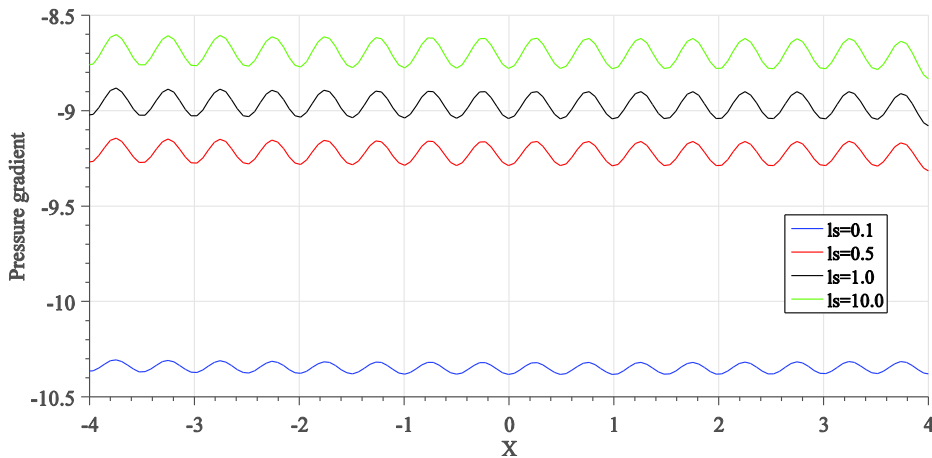


Figure 13. Plot of the pressure gradient (PG) in the X direction with X at $Y = 0.5$ for varying l_s from 0.1 to 10.

The variation of the shear stress on the top wall as shown in Fig. 14 is quite similar to the previous case. Due to the small characteristic length of the patterning, shear stress profiles deviates from the previous case.

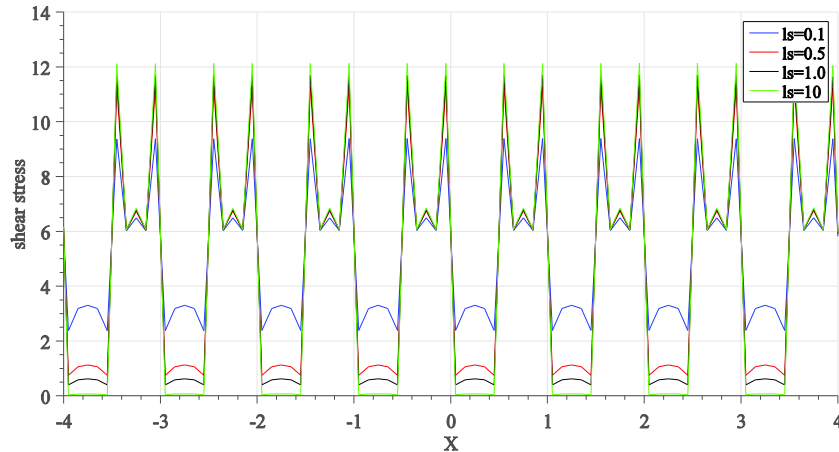


Figure 14. Plot of the shear stress with X at $Y = 1$ for varying l_s from 0.1 to 10.

Conclusions

In this study, flow in out-phase slip-patterned rectangular micro-channels is analyzed using boundary element method (BEM). Two subcases of out-phase slip-patterning namely, large and fine have been discussed. For each of the mentioned cases, the streamline profiles for different values of slip length have been investigated. It was understood that the U and V velocities varies significantly with slip length. It is also observed that the pressure gradient (PG) and wall shear stress have greater dependency over slip-length. When the slip length is very high, it was observed that there is practically no resistance to the flow and therefore shear stress vanishes on the wall.

It is found that the analytical solution is almost not possible for such configuration of boundary conditions. In order to handle such complexities in boundary conditions the presented boundary element solution is very useful.

References

- [1] Nishad, C. S., Chandra, A., Raja Sekhar, G.P. (2016) Flows in slip-patterned micro-channels using boundary element methods, *Engineering Analysis with Boundary Elements* **73** 95–102.
- [2] Hu, S., Ren, X., Bachman, M., Sims, C. E., Li, G., Allbritton, N. (2002) Surface modification of poly (dimethylsiloxane) microfluidic devices by ultraviolet polymer grafting, *Analytical Chemistry* **74** (16) 4117–4123.
- [3] Choi, C.-H., Kim, C.-J. (2006) Large slip of aqueous liquid flow over a nanoengineered superhydrophobic surface, *Physical Review Letters* **96** (6) 066001.
- [4] Lauga, E., Stone, H. A. (2003) Effective slip in pressure-driven Stokes flow, *Journal of Fluid Mechanics* **489** 55–77.
- [5] Kelmanson, M. (1983) An integral equation method for the solution of singular slow flow problems, *Journal of Computational Physics* **51** (1) 139–158.
- [6] Kelmanson, M. (1983) Boundary integral equation solution of viscous flows with free surfaces, *Journal of Engineering Mathematics* **17** (4) 329–343.
- [7] Lu, W.-Q., Chang, H.-C. (1988) An extension of the biharmonic boundary integral method to free surface flow in channels, *Journal of Computational Physics* **77** (2) 340–360.
- [8] Mazouchi, A., Homsy, G. (2001) Free surface Stokes flow over topography, *Physics of Fluids* (1994–present) **13** (10) 2751–2761.

- [9] Mazouchi, A., Gramlich, C., Homsy, G. (2004) Time-dependent free surface Stokes flow with a moving contact line. I. Flow over plane surfaces, *Physics of Fluids* (1994-present) **16** (5) 1647–1659.
- [10] Goodwin, R., Homsy, G. (1991) Viscous flow down a slope in the vicinity of a contact line, *Physics of Fluids A: Fluid Dynamics* (1989-1993) **3** (4) 515–528.
- [11] Krechetnikov, R., Homsy, G. M. (2006) Surfactant effects in the landau–levich problem, *Journal of Fluid Mechanics* **559** 429–450.
- [12] Ingham, D., Yuan, Y. (1997) Multiple solutions of Stokes flow with a free surface, *Engineering Analysis with Boundary Elements* **19** (4) 261–268.
- [13] Pozrikidis, C. (1992) Boundary integral and singularity methods for linearized viscous flow, Cambridge University Press.
- [14] Cheng, A. (2000) Particular solutions of laplacian, helmholtz-type, and polyharmonic operators involving higher order radial basis functions, *Engineering Analysis with Boundary Elements* **24** (7) 531–538.
- [15] Zeb, A., Elliott, L., Ingham, D.B., Lesnic, D. (1998) The boundary element method for the solution of Stokes equations in two-dimensional domains, *Engineering Analysis with Boundary Elements* **22** (4) 317–326.